Conformable Skin Electronics

Based on Spiral Pattern

by

Yiling Fan

A Thesis Presented in Partial Fulfillment
of the Requirements for the Degree
Master of Science

Approved April 2015 by the
Graduate Supervisory Committee:

Hanqing Jiang, Chair
Owen Hildreth
Hongbin Yu

ARIZONA STATE UNIVERISTY

May 2015

ABSTRACT

Skin electronics is one of the most promising applications of stretchable electronics. The versatility of skin electronics can only be guaranteed when it has conformal contact with human skin. While both analytical and numerical solutions for contact between serpentine interconnects and soft substrate remain unreported, the motivation of this thesis is to render a novel method to numerically study the conformability of the serpentine interconnects. This thesis explained thoroughly how to conduct finite element analysis for the conformability of skin electronics, including modeling, meshing method and step setup etc.. User-defined elements were implemented to the finite element commercial package ABAQUS for the analysis of conformability. With thorough investigation into the conformability of Fermat's spiral, it has been found that the kirigami based pattern exhibits high conformability. Since thickness is a key factor to design skin electronics, the thesis also talked about how the change of thickness of the skin electronics impacts on the conformability.

DEDICATION

This thesis is dedicated to my parents who have been supporting me and encouraging me ever since I started my education. Also, many thanks go to my friends who love, inspire and accompany me for all time.

ACKNOWLEDGEMENTS

After all confusion, exhaustion, frustration and skeptic, I am excited and, most importantly, humbly grateful as I accomplished the master's degree, where is just the beginning of the end.

I have been extremely fortunate to work with Prof. Hanqing Jiang, who is decisive, visionary, determined, creative and knowledgeable. Prof. Jiang helped me open the door to the enchanting world of mechanics, and guided me through the rough trip of academy. With his advice and teaching, I have learned to become a considerate person. I am truly grateful to have Prof. Jiang as my program advisor.

My thanks also go to my collogue in ASU, Zeming Song, Wenwen Xu, Teng Ma, Xu Wang and Cheng Lv. They have been helping and supporting me ever since I worked on this project.

Finally, I want to thank Prof. Owen Hildreth and Prof. Hongbin Yu for kindly being the committee members of my thesis program.

TABLE OF CONTENTS

Page

CHAPTER Page

LIST OF TABLE

Table Page

LIST OF FIGURES

CHAPTER 1

INTRODUCTION

1.1 Stretchable Electronics

Stretchable electronics is the so-called electronics that can deform elastically. Unlike traditional rigid electronic devices, stretchable electronics has the capacity of conformably mounting on soft curvilinear environment. Stretchable electronics is of growing attention from scientists and engineers, mainly thanks to its ability to deliver functions that established technologies cannot achieve, including wearable photovoltaics [1], 'epidermal' health/wellness monitors [2], curvilinear digital cameras [3, 4], bio-integrated therapeutic devices [5, 6], and sensitive robotic skins [7-10]. With carefully chosen materials and mechanical design, stretchable electronics exhibits promising features such as twisting like a rope, bending like a rubber, or collapsing like soft cells. What is more appealing is that there is no limit to the rigidity of the employed materials, even brittle materials, if needed, can be complemented into the design. It is also noticeable that even at its highly stretched/deformed state, stretchable electronics shows no sign of mechanical fatigue and insignificant functional change. The common design for stretchable electronics nowadays is of the island-bridge architectures, in which the active components reside at the island and the electrical interconnects form the bridge. In such designs, the serpentine based interconnects play a major role in enhancing stretchability. As for the design code of the stretchable electronics, there are three anticipated goals: (1) the island should fill in the device with filling ratio as high as possible; (2) the bridge is sufficient in length so that it ensures good stretchability; (3) the serpentine based bridge meets the expectation of conformal contact. Researchers have

proposed various types of bridge patterns. Ko proposed an arc-shaped layouts resulting from Euler buckling [3, 4, 11]. Serpentine based bridge is another type of interconnect [2, 12-16]. The design of serpentine traces allows noncoplanar geometries, in either or both the original and deformed state. The most recent studies from Lv has developed a novel interconnect of spiral-shaped pattern [17]. Of all of the serpentine patterns mentioned above, the spiral pattern has shown better stretchability, when filling ratios of the serpentine patterns remain the same. Since the arc-shaped interconnect is comparatively simple, the model has been being thoroughly examined using fundamental mechanics theories [18-20]. The serpentine interconnects are advanced designs for stretchable electronics simply because they provide improved stretchability even with small coverage. However, complex geometries and complicated buckling mechanism make it difficult for theoretical discussion. Finite element method (FEM) was used to investigated the deformation of the serpentine interconnects under tensile forces [14]. Finding the conformability of the serpentine interconnects analytically or numerically is generally complicated. Energy method was used to determine whether conformal contact is true given parameters such as Young's modules and surface roughness etc. [21].

1.2 Mechanics of Skin Electronics

Skin electronics is a significant application of stretchable electronics so far. One of the mostly anticipated features that skin electronics carries is that they are capable of functioning well even under large deformation or frequent human activities. Another important feature skin electronics should be equipped with is the conformability, which takes care of the flexibility of skin electronics. In order to achieve qualified conformability for skin electronics, it is necessary to look at what influences the way skin

electronics is mounted on human skin. While both analytical and numerical solutions for contact between serpentine interconnects and soft substrate remain unreported, the motivation of this thesis is to render a novel method to numerically study the conformability of the serpentine interconnects, which will be covered in Chapter 3. Previous studies have shown that van der Waals forces play a critical role in providing adhesion between skin electronics and skin [42, 43]. Details about how van der Waals forces play into skin electronics will be elaborated in Chapter 3. Cheng and Wang [42, 43] also indicate that the lamination of skin electronics onto skin involves consideration for material properties such as effective bending stiffness, skin roughness, thickness of devices and contact area. Among all of the factors that affect conformability, thickness is of most concern due to the ease with which manufacturers deal with the dimensions of devices. In Chapter 5, the thesis will discuss how conformability of skin electronics responses to the change of thickness of devices.

1.3 Kirigami Based Interconnects

In fact, the spiral pattern was inspired by applying kirigami structures to soft electronics. Kirigami, spread in the SE Asia since 17^{th} century, is an art of cutting and folding paper. As a variation of origami, kirigami structures has received broad attention from artists, mathematicians and architects, largely due to the reason that it has almost all of merits that an origami structure possesses. As far as engineering is concerned, two of the most important features of an origami structure are: the ease to produce a foldable/deployable structure and the provision at the same time of reinforcement function. Deployable structures can be found in [22, 23]. Also, when an origami structure is created from a single flat sheet, this process usually enables one to design a lightweight

but rigid structure [24]. Another significant application of the origami and kirigami structure is in the field of electronics. Researchers have engineered various kinds of kirigami patterns to design stretchable electronics or devices [25, 26]. The motivation of using kirigami pattern for stretchable electronics arises from two factors – good stretchability and superb conformability. To design the kirigami patterns so that they achieve the desired conformability, theoretical analysis has been conducted by using the energy approach to characterize the deformed shapes. Also, I have performed finite element analysis to simulate how well a spiral pattern collapses on a round surface. User-defined spring elements were implemented in commercial finite element package ABAQUS. Simulation results of a spiral pattern that is conformal to a sphere shows that the conformability, defined as the contacted area over total area, could reach as much as 99.7%, while a 2D sheet has 0% conformability.

CHAPTER 2

GEOMETRY AND DESIGN

2.1 Pattern Design

There are many approaches utilized to design stretchable electronics and there are generally two categories. The first approach is to use organic materials that are intrinsically stretchable. However, they suffer with low electrical mobility for high-performance electronics [27-29]. The second approach employs the so-called island-interconnect structure where the inorganic devices are placed on the rigid island while the interconnects are stretchable to make the entire system stretchable [19, 30, 31]. The island-interconnect structures are usually supported by elastomeric substrate and the recent development on foldable electronics has extended this structure to foldable substrate using the concept of paper folding (i.e., origami) [24, 25, 32]. The reason for the design of stretchable interconnects is to improve the stretchability. The interconnects are usually patterned to serpentine shape [31, 33, 34] and recently to semi-similar serpentine shapes [35-37].

The main focus of this thesis lies in the more advanced spiral-based interconnects [17]. So far, two spiral patterns, Fermat's spiral and the golden spiral, are of interest in this study for conformability. Fermat's spiral has mathematical expression in polar coordinate system:

$$r = \pm a\theta^{1/2} \tag{2.1}$$

where a is the scale factor, and θ and r are the polar coordinate variables. The polar equation for a golden spiral can be expressed in such way:

$$r = ae^{b\theta} \tag{2.2}$$

where a is the scale factor, b is the growth factor, and θ and r are the polar coordinate variables. Both patterns are shown in Fig. 1. While Fermat's spiral has an approximately

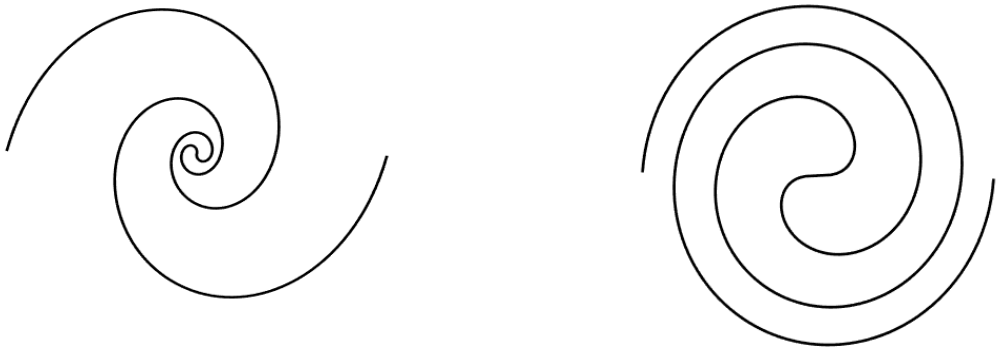

(a) (b)

Fig. 1. Examples of a golden spiral (a) and a Fermat's spiral (b).

equal gap in between spiral stripes, the golden spiral tends to grow increasingly. The design of golden spiral has the advantage of keeping the spiral pattern from overlapping on itself, which will be mentioned in Chapter 5.

2.2 Design Criteria and Constraint

For an island-interconnect type of structure which is in its unstrained state, the majority of the total area should be covered by island components for the purpose of placing as many active components as possible. In this sense, there is only limited space for island components. In the limited area, one interconnect or multiple interconnects can be placed. From the consideration of electrical conductivity, it is advantageous to use multiple interconnects, because the break of one interconnect does not necessarily result in electrical failure of the entire structure.

2.3 Interconnects Inspired by Spiral Pattern

When we look at the nature for spiral structures, there are plenty of them out there, such as a nautilus shell [17]. In fact, some similar designs inspired by spirals can be very spontaneous (see Fig. 2). These designs are all constructed in a resembling way that they form a pattern by stemming from the origin and developing alone a path that is based on regular geometric figures such as rectangular and triangle. Thus, one is able to customize a spiral based bridge with various geometries so as to meeting different design codes.

Take the spiral in rectangular shape as an example. The pattern in Fig. 2 (a) is suitable for devices that require a bridge space to be square. One of the significant merits of this design is that this pattern can fit into a square space with the biggest filling ratio possible. The large filling ratio thus results in better stretchability, which makes it a preferred design as the bridge of stretchable electronics. Similar argument also holds for other spiral based serpentines (see Fig. 2 (b)).

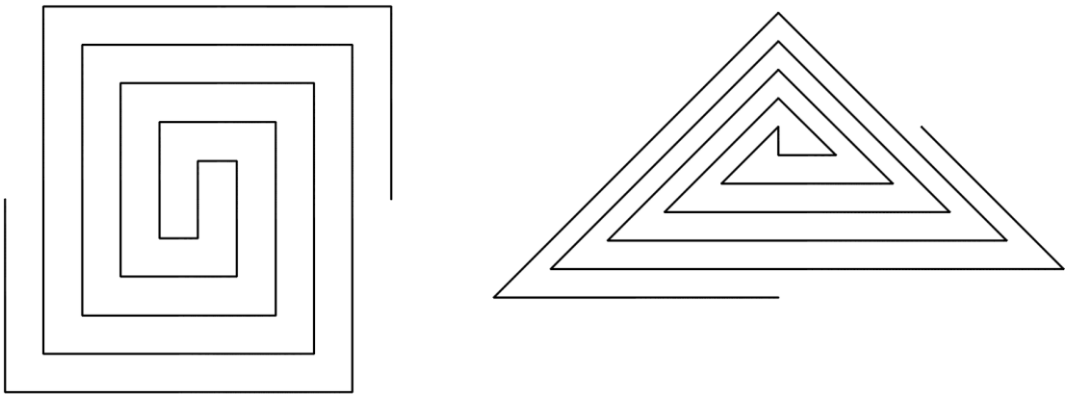

(a) (b)

Fig. 2. Spiral based serpentines. (a) Spiral based serpentine with rectangles as the constructed elements. (b) Spiral based serpentine with triangles as the constructed elements.

CHAPTER 3

FINITE ELEMENT ANALYSIS FOR CONFORMABILITY

3.1 Introduction

3.1.1 Modeling of Stretchable Electronics for Conformability

When we think of placing a thin film on top of a curvilinear substrate, it is imaginable that the film and the substrate will contact firstly at places where distances between and film and the substrate (collapse distance) are shorter. It becomes apparent in the case shown in Fig. 3.

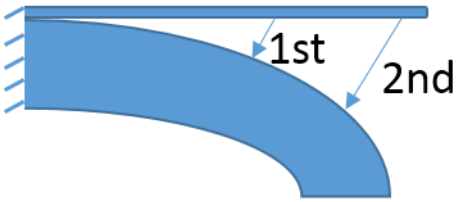

Fig. 3. Conceptual experiment of a thin film collapses on a substrate.

Assume that every infinitesimal area on the thin film is going to be in contact with a counter-area that is equally small on the substrate. And the work of adhesion for each pair of the elements will be the same provided that the materials of both layers are homogeneous. Imagine that a virtual spring is used to connect each pair of the areas. If we think of the potential of the springs as a conversion of energy from surface energy to spring potential, then each of the springs should have the same amount of potential energy regardless of the elongation of the spring. We may also justify the energy conversion by saying that a spring that has a shorter elongation (collapse distance) tends to be stiffer, or the stiffness of the springs differs from one another depending on the

length of the collapse distance, which (1) satisfies the condition of equal potential energy for each spring element and (2) induces a stronger collapse tendency.

As a result, a model was constructed in a manner that a thin film and a substrate were connected to each other by a series of conceptual springs (see Fig. 4). For the convenience of later analysis, the spring elements were designed to pass through the same point that was below the substrate, and the equilibrium distances of the spring elements were set to the length of the part that was below the substrate. Illustration of this model setup will be elaborated in the flowing Chapters. Further derivation for the equilibrium distance is given in Appendix A.

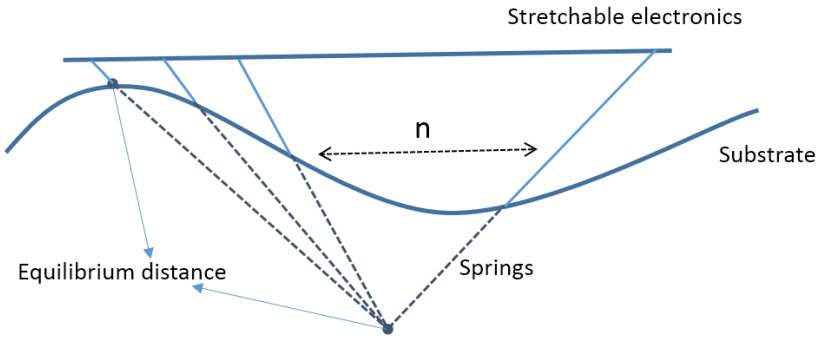

Fig. 4. Modeling of stretchable electronics in contact with a substrate.

3.1.2 Van der Waals forces for skin electronics

Van der Waals forces are one of the many forces that hold matters together. In fact, van der Waals forces are the attractive or repulsive forces between molecular entities (or between groups within the same molecular entity) other than those due to bond formation or to the electrostatic interaction of ions or of ionic groups with one another or with neutral molecules [28]. While van der Waals forces are common in the study of formulation of gases, they also give rise to an attractive force between two solid objects separated by a small gap, which is important in adhesion and in the stability of

colloids [40]. In the beginning, let us take a look at the potential energy associated with van der Waals forces. The energy between two atoms of distance r due to van der Waals forces are usually represented by the Lennard - Jones 6 -12 potential,

$$V(r) = 4\varepsilon\left(\frac{\sigma^{12}}{r^{12}} - \frac{\sigma^{6}}{r^{6}}\right) \tag{3.1}$$

where $\sqrt[6]{2}\sigma$ is the equilibrium distance between the atoms, ε is the bond energy at the equilibrium distance [38]. By denoting the equilibrium distance as $r_0 = \sqrt[6]{2}\sigma$, we are able to rewrite the relationship,

$$V(r) = \varepsilon\left(\frac{r_0^{12}}{r^{12}} - \frac{2r_0^{6}}{r^{6}}\right) \tag{3.2}$$

As can be seen, the distance r between two particles is the only parameter in the function of potential. Thus it is advantageous to plot the function with respect to r and $V(r)$ (see Fig. 5). We can tell from the curve that the potential reaches its minimum state at the equilibrium distance. It is also noticeable that the curve in Fig. 5 shows steeper slope when $r < r_0$, which means that the particles are subjected larger pull-back force when their distance is smaller than the equilibrium distance, which keeps the interconnects from intersecting with the substrate in the view of energy. As the principle of stationary energy states, a structure or body shall deform or displace to a position that minimizes the total potential energy, which means that the thin film, when subjected to van der Waals forces, tends to deform in the direction of every molecule of the film reaching its own equilibrium distance. This indicates a way to investigate whether the thin film has conformal contact with the substrate by manipulating the equilibrium distance.

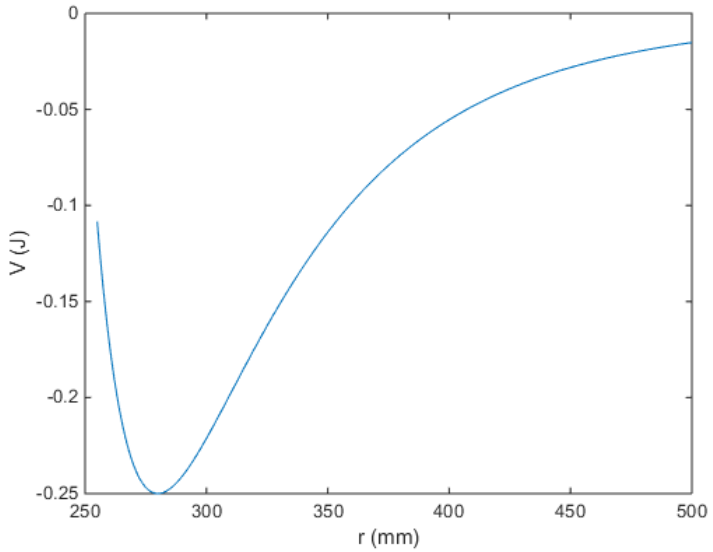

Fig. 5. A plot of Lennard - Jones 6 -12 potential with $r_0 = 280mm$ and $\varepsilon = 1J$ as the selected parameters.

Next let us turn to surface energy. For two known materials in contact, the work of adhesion is given by $g = g_1 + g_2 - g_{12}$, where γ_1 and γ_2 are the surface energy density of the contacting materials respectively, and γ_{12} is the surface energy density of the interfaces. With energy density, we are able to calculate the surface energy in such way

$$U = \gamma b \tag{3.3}$$

where b is the area of the contact.

The thickness of the stretchable electronics is small, though, it is still large enough in the microscopic view, which makes the dominant attractive forces between the stretchable electronics and the substrate is van der Waals forces. For the study of skin electronics, we can assume van der Waals forces are accounted for the surface energy between the stretchable electronics and the substrate. With that it is possible now to relate the potential energy associated with van der Waals forces to surface energy if materials in contact are known. Using the model shown in Fig. 4 and assuming that every spring

element has the same amount of potential energy, we are able to establish a relation for spring element i by combining equation (3.3) and (3.2),

$$\gamma b / n = \varepsilon_i \left(\frac{r_{0i}^{12}}{r^{12}} - \frac{2r_{0i}^{6}}{r^{6}} \right) \tag{3.4}$$

where n is the number of spring elements applied. Note that the spring elements used here are not linear but associated to the potential energy due to van der Waals forces. Also for each spring element, they have different equilibrium distances. Here we can consider ε as the spring stiffness

$$\varepsilon_i (r) = \frac{\gamma b}{n\left(\frac{r_{0i}^{12}}{r^{12}} - \frac{2r_{0i}^{6}}{r^{6}} \right)} \tag{3.5}$$

Note that his user-defined spring does not have a constant stiffness, which is a function in terms of the spring length.

3.2 Pre-processing

The spiral pattern used for conformability study was based on Fermat's spiral, represented by equation (2.1). The spiral was design with $a = 40$ and θ ranging from 0 to 3π (see Fig. 6). With these settings, we are able to construct a spiral in which the distance between two ends reaches 180 (dimensionless). I later assigned the spiral with a unit of micron and then set the thickness of the spiral to $1\mu m$ in the initial analysis.

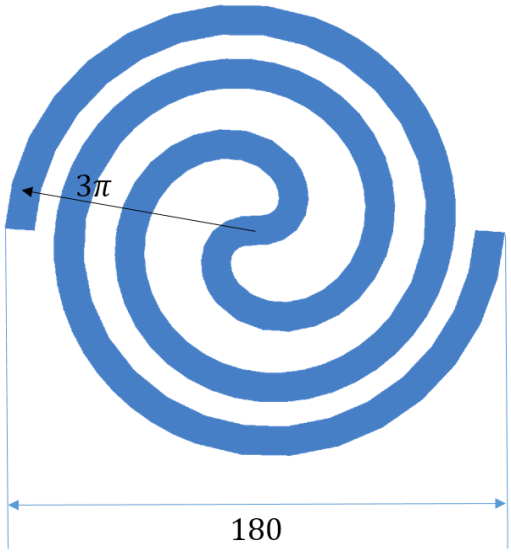

Fig. 6. Fermat's spiral with $a = 40$ and $\theta = [0, 3\pi]$.

The material used for interconnects of skin electronics is normally copper, which has good conductivity and does little/no harm to human skin. The material properties of copper and skin are shown in table 1. It is noticeable that the surface energy of copper is significantly larger than that of skin. Based on equation (3.3) which gives the work of adhesion, we can assume here the surface energy of copper plays a dominant part in determining the work of adhesion. Another important assumption made here was that when skin electronics is mounted, the mechanical response of human skin is negligible because skin is much thicker in size than skin electronics, which is normally in micro scale, regardless of the big difference of Young's modulus.

Table 1
Material Properties of Copper and Human Skin

Materials	Young's Modulus	Poisson Ratio	Surface Energy
Copper	120 Gpa	0.34	1.94 J/m^{-2} [a]
Skin	32.9 kPa [b]	0.3 [b]	42.3 mJ/m^{-2} [c]

Source: a [44]; b [45]; c [46].

3.3 Formulation of the User-defined Spring Elements

In order to simulate van der Waals forces, novel user-defined spring elements were implemented in commercial finite element package ABAQUS. The two-node user-defined spring element (USE) has an original length depending on the equilibrium distance. The potential energy function of the USE was constructed in a way that was discussed in Chapter 3.1.2. The user-defined element was implemented using ABAQUS subroutine UEL. ABAQUS user subroutine UEL [41]

- will be called for each element that is of a general user-defined element type (i.e., not defined by a linear stiffness or mass matrix read either directly or from results file data) each time element calculations are required; and
- (or subroutines called by user subroutine UEL) must perform all of the calculations for the element, appropriate to the current activity in the analysis.

The external loading of the USE is self-provided depending on the elongation of the spring element. Another factor to complete the formulation of the USE is to give the stiffness matrix of the USE. Details of obtaining the external loading and the stiffness matrix for user-defined spring element (USE) will be given below. Getting started, we need to compute the distance between two ends of the spring elements. According to the

setup illustrated in Fig. 4, in which the end node that is below the substrate is fixed, we are able to calculate the distance by

$$r = \left(x - x_0\right)^2 + \left(y - y_0\right)^2 + \left(z - z_0\right)^2 \tag{3.6}$$

where x_0, y_0, z_0 are the coordinates of the fixed end. Take the derivative of r with respect to x, y, z, we have

$$\frac{dr}{dx_i} = \frac{x_i - x_0}{r} \tag{3.7}$$

Get external loading is computed by taking derivative of the potential energy with respect to x, y, z

$$f_i^{ext} = \frac{\partial V}{\partial x_i} = \frac{\partial V}{\partial r}\frac{\partial r}{\partial x_i} = \frac{1}{r}\frac{\partial V}{\partial r}\left(x_i - x_0\right) = L_1\left(V\right)\left(x_i - x_0\right) \tag{3.8}$$

where $i = 1,2,3$ is the tensor notation. The first differential operator was defined as $L_1 = \frac{1}{r}\frac{\partial}{\partial r}$. By taking the derivative of the potential energy in terms of x, y, z further on, we have the stiffness matrix

$$\begin{aligned} K_{ij} &= \frac{\partial^2 V}{\partial x_i \partial x_j} = \frac{\partial}{\partial x_j}\left[\frac{1}{r}\frac{\partial V}{\partial r}\left(x_i - x_0\right)\right] = \frac{1}{r}\frac{\partial V}{\partial r}\delta_{ij} + \left(x_i - x_0\right)\frac{\partial}{\partial x_j}\left(\frac{1}{r}\frac{\partial V}{\partial r}\right) \\ &= \frac{1}{r}\frac{\partial V}{\partial r}\delta_{ij} + \frac{\partial}{\partial r}\left(\frac{1}{r}\frac{\partial V}{\partial r}\right)\frac{\partial r}{\partial x_j}\left(x_i - x_0\right) \\ &= \frac{1}{r}\frac{\partial V}{\partial r}\delta_{ij} + \left(-\frac{1}{r^2}\frac{\partial V}{\partial r} + \frac{1}{r}\frac{\partial^2 V}{\partial r^2}\right)\frac{1}{r}\left(x_j - x_0\right)\left(x_i - x_0\right) \\ &= L_1\left(V\right)\delta_{ij} + L_2\left(V\right)\left(x_i - x_0\right)\left(x_j - x_0\right) \end{aligned} \tag{3.9}$$

where δ_{ij} is the Kronecker delta. Notice that the second differential operator was defined as

$$L_2 = \left(-\frac{1}{r^3}\frac{\partial}{\partial r} + \frac{1}{r^2}\frac{\partial^2}{\partial r^2}\right) \tag{3.10}$$

Apply the differential operators defined earlier to the potential energy function expressed by equation (3.2)

$$L_1(V) = \frac{1}{r}\frac{\partial V}{\partial r} = 12\varepsilon\left(\frac{r_0^6}{r^8} - \frac{r_0^{12}}{r^{14}}\right) \tag{3.11}$$

$$L_2(V) = \left(-\frac{1}{r^3}\frac{\partial V}{\partial r} + \frac{1}{r^2}\frac{\partial^2 V}{\partial r^2}\right) = 24\varepsilon\left(\frac{7r_0^{12}}{r^{16}} - \frac{4r_0^6}{r^{10}}\right) \tag{3.12}$$

With $L_1(V)$ and $L_2(V)$, we are able to derive (1) the external forces in the form,

$$f_i^{ext} = \frac{\partial V}{\partial x_i} = \frac{\partial V}{\partial r}\frac{\partial r}{\partial x_i} = \frac{1}{r}\frac{\partial V}{\partial r}(x_i - x_0) = L_1(V)(x_i - x_0) = 12\varepsilon\left(\frac{r_0^6}{r^8} - \frac{r_0^{12}}{r^{14}}\right)(x_i - x_0) \tag{3.13}$$

and (2) the stiffness matrix in the form,

$$\begin{aligned} K_{ij} &= \frac{\partial^2 V}{\partial x_i \partial x_j} = L_1(V)\delta_{ij} + L_2(V)(x_i - x_0)(x_j - x_0) \\ &= 12\varepsilon\left(\frac{r_0^6}{r^8} - \frac{r_0^{12}}{r^{14}}\right)\delta_{ij} + 24\varepsilon\left(\frac{7r_0^{12}}{r^{16}} - \frac{4r_0^6}{r^{10}}\right)(x_i - x_0)(x_j - x_0) \end{aligned} \tag{3.14}$$

All the derivation performed used tensor notation for the purpose of convenience. Free indices i and j represent the space coordinate ranging from 1 to 3. Another important feature of both the external forces and the stiffness matrix is that they are solely dependent on the elongation of the spring elements, which gives rise to significant simplification to the finite element analysis for conformability study.

3.4 Mesh

Meshing of the spiral is extremely important to gain an accurate solution for the analysis proposed by this thesis. First of all, we should know for fact that the attractive force due to van der Waals forces between two homogenous surfaces is uniformly distributed. Since the attractive force between the stretchable electronics and the substrate was simulated using spring elements, uniform interaction means that the spring elements should be uniformly connected to the spiral based interconnect. Because the spring elements share nodes with elements on the spiral pattern, the meshing on the spiral

pattern should contain structured elements so that a uniform distribution of the spring elements is satisfied. For better mesh quality, quadrilateral elements (Q4) are preferred.

However, due to the complicated geometric design of the spiral based interconnect, it is sometimes difficult to achieve structured meshing. In order to obtain desired mesh, user modification of the mesh is usually necessary. In ABAQUS, meshing the spiral based interconnect by structured mesh control would seem unlikely due to the complex geometry. An alternative method would be applying partition to divide the model into several parts. Also, for those areas that require triangle elements due to complicated geometry, users would have to modify the seeding location for a proportional distribution of nodes. Comparison between the mesh using free meshing method and the mesh method involving model partition is shown in Fig. 7. The mesh in Fig. 7 (b) is clearly much more structured than the mesh shown in Fig. 7 (a). In the free mesh, there is poor illustration of keeping the sizes of the elements consistent, whereas the elements in Fig. 7 (b) have similar sizes. However, bad mesh quality could still be seen in the area where geometry of the spiral involves large curvature, such as the center of the spiral pattern in Fig. 7 (b). For finite element analysis conducted for the study of conformability, stress is not the biggest concern, which means that there is no need to refine the mesh in area triggering high stress. In fact, a refinement of mesh to get accurate stress representation is indeed against what has been suggested for an optimal mesh of the conformability study. Tests also showed improvement of computational speed for structured mesh. However, a polymer microcable structure may be introduced to reduce to stress concentration effect [47].

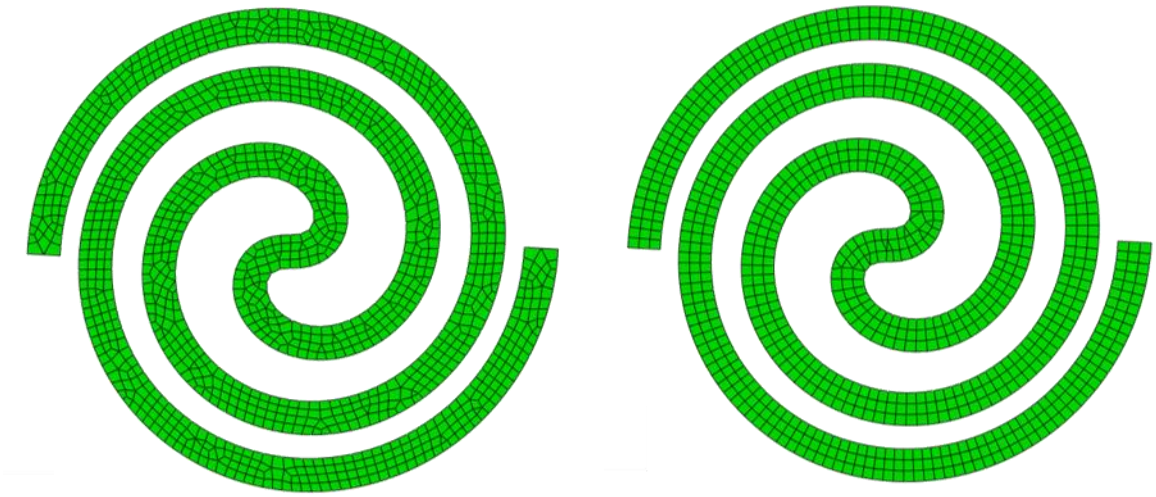

(a) (b)

Fig. 7. Mesh comparison. (a) Mesh by free meshing method. (b) Mesh involving model partition.

One way to determine the quality of the mesh is to visually observe the part. However, it is of necessity to provide a method capable of accurately determining the mesh quality. A term called density of nodes was defined here, which is given by

$$\beta = \frac{n}{T} \tag{3.15}$$

where β is the density of nodes, n is the number of nodes in an identical amount of closed area which is randomly selected, and T represents the total number of nodes. For a valid selection of mesh, β needs to be about the same value.

3.5 Procedures

When analyzing interconnects of the skin electronics on a substrate with small curvilinear shape, a convergent analysis appears likely with a direct application of spring elements. The case would be different, though, when we need to deal with analysis that requires large deformation of the interconnects. For large deformation analysis, it is

advantageous then to break down the entire collapse into several steps, in every one of which the deformation remains small enough for convergence. The finite element analysis conducted in this thesis involved a substrate of the half-sphere shape. Staring at an undeformed state that is a planar pattern, the spiral based interconnects are supposed to deform such that it has conformal contact with the substrate. This entire contact procedure requires very large deformation so separate steps are indispensable. In order to achieve a final state that the spiral based interconnects wrap around the sphere substrate, we may get it deform on a substrate with smaller height in the first place. By updating the deformation and getting it again deform onto the next substrate that has steeper surface, we will eventually finalize it with an expected contact. For the analysis performed in this thesis, the steps of contact of the spiral pattern were shown in Fig. 8.

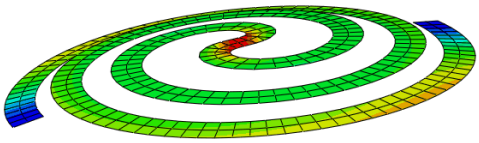

Fig. 8 (a)

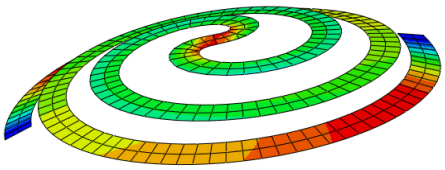

Fig. 8 (b)

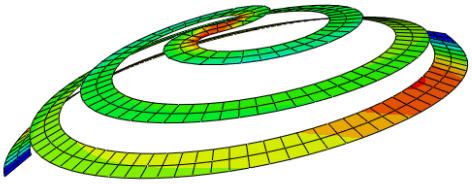

Fig. 8 (c)

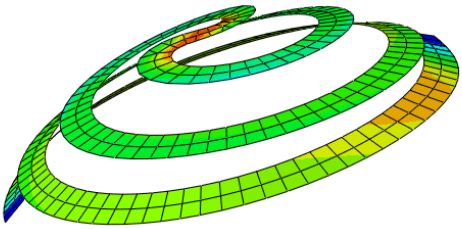

Fig. 8 (d)

Fig. 8. Deformation flow of the spiral. (a), (b), (c) and (d) represent the deformation at 25%, 50%, 75% and 100% respectively.

CHAPTER 4

CONFORMABILITY

Conformability is one of the major concerns of skin electronics. There are two categories of contact status, one of which is called sustainable contact, while the other one is called intimate contact. Sustainable contact is relatively easy to achieve since it only requires that skin electronics adhere to human skin with or without allowed interference. The intimate contact is a higher level of contact type, which requires that skin electronics conform to the uneven skin. The intimate contact is a desired level of contact for skin electronics. This is because skin electronics is typically used to measure body vitals, which can be accessible with accuracy and sensitivity only when intimate contact occurs.

This thesis measured the conformability in the sense of intimate contact, so the goal here is to see what proportion of the interconnects eventually collapses onto the substrate. With the final state of deformation, the research measured the conformability, which is the contacted area over the total area, by comparing the nodes on the interconnects with the spherical function. If a node of the interconnects is separated from the substrate surface by a tolerance distance, which is decided upon the size of model, we say this node is in contact with the substrate. By counting the number of nodes that are on the substrate by a tolerance distance, we can calculate the conformability in the following form,

$$c = \frac{n}{N} \tag{4.1}$$

where c is variable approximately equal to the actual conformability, n is the number of nodes in contact and N is the total number of nodes. A Matlab program was developed to count the number of nodes in contact, and thereafter solve for the conformability (See Appendix B).

CHAPTER 5

RESULTS

The final state of contact for the spiral pattern is shown in Fig. 9. As can be seen from Fig. 9, the spiral pattern conforms to the spherical substrate with a trend of moving towards the center. Some parts, especially at the ending of the spiral pattern, have overlapped upon other stripe. In cases where one tries to avoid those overlapping occasions, there is a need to set the outer stripe further away from the inner one. So a design based on the golden spiral would be an alternative solution to the circumstances of overlapping.

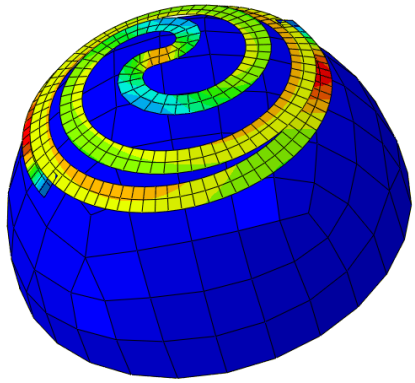

Fig. 9. A spiral pattern in contact with a spherical substrate with high conformability.

By using the program in Appendix B, a conformability of 99.7% for Fermat's spiral was detected. The high conformability indicates that Fermat's spiral, as a kirigami pattern, is suitable to be the interconnects of skin electronics. In fact, thickness is also a significant parameter for the conformability of skin electronics. An increase of thickness of skin electronics usually gives rise to an unproportional lost in conformability. Reportedly, for FS made of polyimide-gold, the skin roughness for conformal contact

decreases from $\sim 56\mu m$ to $\sim 30\mu m$ as the device thickness increases by 8 times [44]. Though a thick device ensures a qualified strength, it is obviously better to design skin electronics as thin as possible for the sake of wearing comfort and conformal contact. It has been reported that there exists a critical thickness for a specific design of skin electronics [43]. What is meant by the critical thickness is that when the thickness of skin electronics exceeds this critical value, it is unlikely for the devices to have conformal contact with human skin. The critical thickness is usually obtained by experimental methods. Here finite element analysis was performed to study the change of conformability in terms of the thickness. The trend of conformability is shown in Fig. 10. For a skin device thinner than $1.2\mu m$, it has conformal contact with human skin. Yet the conformability of skin electronics decreases dramatically with the increase of device thickness, and the conformability hits 28% as the device thickness reaches $4\mu m$. Actually the simulation results agree well with experimental data, which indicated that for devices thicker than $1.2\mu m$, the contact pressure will reach $20Kpa$, a level that starts causing human discomfort and a sign of weak lamination [31]. When the thickness rises to as high as $3.8\mu m$, experiments revealed that skin electronics would lose conformal contact to human skin.

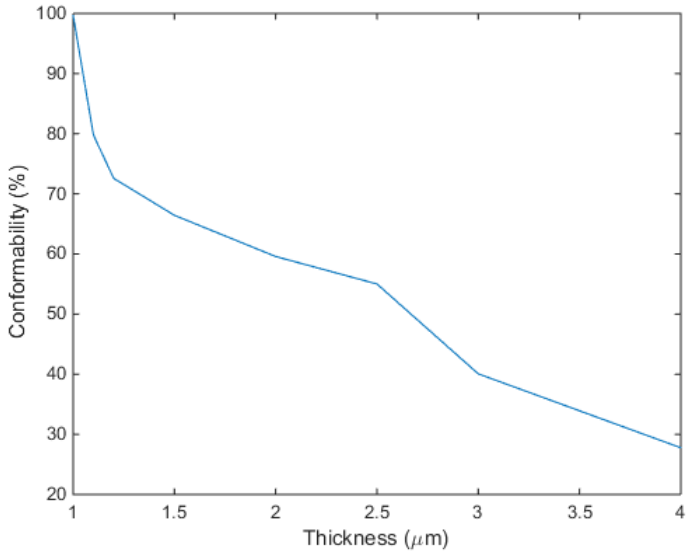

Fig. 10. Thickness vs conformability.

CHAPTER 6

CONCLUSION

This thesis addressed the validity of spiral based patterns being used to form the bridge of skin electronics, and have thoroughly discussed Fermat's spiral in terms of conformability. In the analysis of conformability for Fermat's spiral, we assumed the potential of van der Waals forces was the driven forces for the work of adhesion, for reasons (1) van der Waals forces formed the major attractive force between two solid objects separated by a small gap [39]; and (2) large pull-back forces will be induced for a molecule distance shorter than the equilibrium distance, which keeps the interconnects from intersecting with the substrate. The usage of user-defined spring elements, which employ the potential function due to van der Waals forces, successfully captured the deformation of the spiral pattern and subsequently obtained conformability of 99.7% for Fermat's spiral (thickness = $1\mu m$) placed on top of a spherical substrate. The thesis also discussed extensively how the change of thickness of skin electronics could affect the conformability. Simulation results revealed that the optimal thickness should be less than $1.2\mu m$, which on one hand causes little irritation to human skin, and on the other hand ensures high conformability.

CHAPTER 7

FUTURE WORK

We now know that for a thin device of skin electronics, it is likely for the device to have conformal contact with human skin, if the design of interconnects is legitimate. However, there are a lot of factors that affect how well skin electronics is mounted on human skin, including the skin roughness, materials used for skin electronics and the skin wrinkle effect.

As far as skin roughness is concerned, both aging skin and hairy skin appear rougher. With rough skin, conformal contact takes more surface energy than usual to happen, because conformal contact with rough skin needs large deformation [42]. Hence, there is a need to involve skin roughness in the simulation for conformability.

Three material properties, electrical conductivity, Young's modulus and surface energy, are very important to construct skin electronics. Good conductivity ensures secure electrical connection with low energy consumption. Since skin electronics is usually in the micron scale, the power system in the device is relatively small in space as well, which provides very limited battery life. Therefore, an energy efficient feature is needed for a device to last an anticipated active time. We can see Young's modulus and surface energy as a combination of properties that impact on the conformability of skin electronics. High Young's modulus makes the skin electronics harder to deform; and high surface energy results in a bigger tendency to have conformal contact. Therefore, the optimal material should meet the requirements of good electrical conductivity, low Young's modulus and high surface energy.

The last consideration for skin electronics would be involving human activities in post conformability test. Since human skin is very soft and deformable, large amount of human activities can give rise to a significant change of the shape of skin surface, which consequently impacts the way that skin electronics collapse onto the skin surface. Theoretically speaking, when the skin electronics moves along with skin electronics due to human activities, the deform shape of the skin electronics also changes, giving a configuration that contains different strain energy due to deformation. Future work should look into the physics behind the deformation of human skin and then simulate how the spiral patterns are going to react to the skin deformation.

REFERENCE

[1] Yoon, Jongseung, et al. "Ultrathin silicon solar microcells for semitransparent, mechanically flexible and microconcentrator module designs." *Nature materials*7.11 (2008): 907-915.

[2] Kim, Dae-Hyeong, et al. "Epidermal electronics." *science* 333.6044 (2011): 838-843.

[3] Ko, Heung Cho, et al. "A hemispherical electronic eye camera based on compressible silicon optoelectronics." *Nature* 454.7205 (2008): 748-753.

[4] Shin, Gunchul, et al. "Micromechanics and Advanced Designs for Curved Photodetector Arrays in Hemispherical Electronic-Eye Cameras." *Small* 6.7 (2010): 851-856.

[5] Timko, Brian P., et al. "Electrical recording from hearts with flexible nanowire device arrays." *Nano letters* 9.2 (2009): 914-918.

[6] Viventi, Jonathan, et al. "A conformal, bio-interfaced class of silicon electronics for mapping cardiac electrophysiology." *Science translational medicine* 2.24 (2010): 24ra22-24ra22.

[7] Wagner, Sigurd, et al. "Electronic skin: architecture and components." *Physica E: Low-dimensional Systems and Nanostructures* 25.2 (2004): 326-334.

[8] Someya, Takao, et al. "A large-area, flexible pressure sensor matrix with organic field-effect transistors for artificial skin applications." *Proceedings of the National Academy of Sciences of the United States of America* 101.27 (2004): 9966-9970.

[9] Mannsfeld, Stefan CB, et al. "Highly sensitive flexible pressure sensors with microstructured rubber dielectric layers." *Nature materials* 9.10 (2010): 859-864.

[10] Takei, Kuniharu, et al. "Nanowire active-matrix circuitry for low-voltage macroscale artificial skin." *Nature materials* 9.10 (2010): 821-826.

[11] Lee, Jongho, et al. "Stretchable GaAs photovoltaics with designs that enable high areal coverage." *Advanced Materials* 23.8 (2011): 986-991.

[12] Kim, Dae-Hyeong, et al. "Materials and noncoplanar mesh designs for integrated circuits with linear elastic responses to extreme mechanical deformations." *Proceedings of the National Academy of Sciences* 105.48 (2008): 18675-18680.

[13] Kim, Dae-Hyeong, et al. "Ultrathin Silicon Circuits With Strain-Isolation Layers and Mesh Layouts for High-Performance Electronics on Fabric, Vinyl, Leather, and Paper." *Advanced Materials* 21.36 (2009): 3703-3707.

[14] Kim, Dae-Hyeong, et al. "Optimized structural designs for stretchable silicon integrated circuits." *Small* 5.24 (2009): 2841-2847.

[15] Kim, Rak-Hwan, et al. "Materials and Designs for Wirelessly Powered Implantable Light-Emitting Systems." *Small* 8.18 (2012): 2812-2818.

[16] Li, Teng, et al. "Compliant thin film patterns of stiff materials as platforms for stretchable electronics." *Journal of materials research* 20.12 (2005): 3274-3277.

[17] Lv, Cheng, Hongyu Yu, and Hanqing Jiang. "Archimedean spiral design for extremely stretchable interconnects." *Extreme Mechanics Letters* (2014): 29-34.

[18] Jiang, Hanqing, et al. "Post-buckling analysis for the precisely controlled buckling of thin film encapsulated by elastomeric substrates." *International Journal of Solids and Structures* 45.13 (2008): 2014–2023.

[19] Song, J., et al. "Mechanics of noncoplanar mesh design for stretchable electronic circuits." *Journal of Applied Physics* 105.12 (2009): 123516.

[20] Su, Yewang, et al. "Postbuckling analysis and its application to stretchable electronics." *Journal of the Mechanics and Physics of Solids* 60.3 (2012): 487-508.

[21] Wang, Shuodao, et al. "Mechanics of epidermal electronics." *Journal of Applied Mechanics* 79.3 (2012): 031022.

[22] Pellegrino, Sergio, ed. *Deployable structures*. No. 412. Springer Science & Business Media, 2002.

[23] Mitsuishi, M., et al.. "41th Conference on Manufacturing Systems." *Proceedings of the 41th CIRP Conference of Manufacturing Systems.* Tokyo, 26-28 May.

[24] Lv, Cheng, et al. "Origami based mechanical metamaterials." *Scientific reports*4 (2014).

[25] Song, Zeming, et al. "Origami lithium-ion batteries." *Nature communications* 5 (2014).

[26] Wang, Xu, et al. "Kirigami-based stretchable lithium-ion batteries." *Scientific Report* (in press).

[27] Garnier, Francis, et al. "All-polymer field-effect transistor realized by printing techniques." *Science* 265.5179 (1994): 1684-1686.

[28] Crone, B., et al. "Large-scale complementary integrated circuits based on organic transistors." *Nature* 403.6769 (2000): 521-523.

[29] Kelley, Tommie W., et al. "Recent progress in organic electronics: Materials, devices, and processes." *Chemistry of Materials* 16.23 (2004): 4413-4422.

[30] Khang, Dahl-Young, et al. "A stretchable form of single-crystal silicon for high performance electronics on rubber substrates." *Science* 311.5758 (2006): 208-212.

[31] Kim, Dae-Hyeong, et al. "Materials and noncoplanar mesh designs for integrated circuits with linear elastic responses to extreme mechanical deformations." *Proceedings of the National Academy of Sciences* 105.48 (2008): 18675-18680.

[32] Tang, Rui, et al. "Origami-enabled deformable silicon solar cells." *Applied Physics Letters* 104.8 (2014): 083501.

[33] Widlund, Thomas, et al. "Stretchability and compliance of freestanding serpentine-shaped ribbons." *International Journal of Solids and Structures*51.23 (2014): 4026-4037.

[34] Zhang, Yihui, et al. "A hierarchical computational model for stretchable interconnects with fractal-inspired designs." *Journal of the Mechanics and Physics of Solids* 72 (2014): 115-130.

[35] Fan, Jonathan A., et al. "Fractal design concepts for stretchable electronics."*Nature communications* 5 (2014).

[36] Zhang, Yihui, et al. "Mechanics of ultra-stretchable self-similar serpentine interconnects." *Acta Materialia* 61.20 (2013): 7816-7827.

[37] Xu, Sheng, et al. "Stretchable batteries with self-similar serpentine interconnects and integrated wireless recharging systems." *Nature communications* 4 (2013): 1543.

[38] Jiang, L. Y., et al. "A cohesive law for carbon nanotube/polymer interfaces based on the van der Waals force." *Journal of the Mechanics and Physics of Solids* 54.11 (2006): 2436-2452.

[39] McNaught, Alan D., et al. *Compendium of chemical terminology*. Vol. 1669. Oxford: Blackwell Science, 1997.

[40] Winterton, R. H. S. "Van der Waals forces." *Contemporary Physics* 11.6 (1970): 559-574.

[41] Hibbitt, Karlsson, and Sorensen. *ABAQUS/Standard user's manual*. Vol. 1. Hibbitt, Karlsson & Sorensen, 2001.

[42] Wang, Shuodao, et al. "Mechanics of epidermal electronics." *Journal of Applied Mechanics* 79.3 (2012): 031022.

[43] Cheng, Huanyu, and Shuodao Wang. "Mechanics of Interfacial Delamination in Epidermal Electronics Systems." *Journal of Applied Mechanics* 81.4 (2014): 044501.
[44] Vitos, Levente, et al. "The surface energy of metals." *Surface Science* 411.1 (1998): 186-202.

[45] Delalleau, Alexandre, et al. "Characterization of the mechanical properties of skin by inverse analysis combined with the indentation test." *Journal of biomechanics* 39.9 (2006): 1603-1610.

[46] Mavon, A., et al. "Changes in sebum levels and skin surface free energy components following skin surface washing." *Colloids and Surfaces B: Biointerfaces* 10.5 (1998): 243-250.

[47] Kim, Eric, et al. "A robust polymer microcable structure for flexible devices." *Applied Physics Letters* 102.3 (2013): 033506.

APPENDIX A

DERIVATION OF EQUILIBRIUM DISTANCE

Derivation of the equilibrium distance is given upon an ellipsoid model (see Fig. S1), which was used as the shape of a substrate.

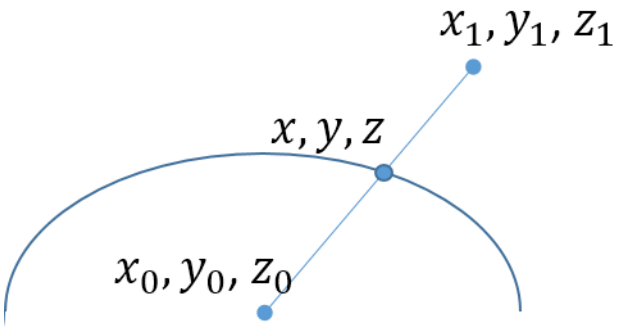

Fig. S1. Diagram of a substrate and a spring element.

The equilibrium distance is the line segment between node (x_0, y_0, z_0) and node (x, y, z). While the location of node (x_0, y_0, z_0) is fixed. The coordinate of node (x_1, y_1, z_1) is given and updated by the nodal displacement of the spiral pattern. With the function of the ellipsoid being known, we are able to solve for the coordinate of node (x, y, z).

The line equation specified by node (x_0, y_0, z_0) and node (x, y, z) can be expressed in the form

$$\frac{x - x_0}{x_1 - x_0} = \frac{y - y_0}{y_1 - y_0} = \frac{z - z_0}{z_1 - z_0} \tag{S1.1}$$

The equation of an ellipsoid is represented by

$$\frac{(x - x_0)^2}{a^2} + \frac{(y - y_0)^2}{b^2} + \frac{(z - z_0)^2}{c^2} = 1 \tag{S1.2}$$

Write out y and z in terms of x ,

$$y = \frac{(x - x_0)(y_1 - y_0)}{x - x_0} + y_0$$
$$z = \frac{(x - x_0)(z_1 - z_0)}{x - x_0} + z_0 \tag{S1.3}$$

Plug in y and z to the ellipsoid function,

$$\frac{(x - x_0)^2}{a^2} + \frac{(x - x_0)^2 (y - y_0)^2}{b^2 (x_1 - x_0)^2} + \frac{(x - x_0)^2 (z - z_0)^2}{c^2 (x_1 - x_0)^2} = 1 \tag{S1.4}$$

Equation (S1.4) gives the relation,

$$(x - x_0)^2 = \frac{a^2 b^2 c^2 (x_1 - x_0)^2}{b^2 c^2 (x_1 - x_0)^2 + a^2 c^2 (y_1 - y_0)^2 + a^2 b^2 (z_1 - z_0)^2} \tag{S1.5}$$

Applying similar process to y and z, we are able to get the other two relations,

$$(y - y_0)^2 = \frac{a^2 b^2 c^2 (y_1 - y_0)^2}{b^2 c^2 (x_1 - x_0)^2 + a^2 c^2 (y_1 - y_0)^2 + a^2 b^2 (z_1 - z_0)^2}$$
$$(z - z_0)^2 = \frac{a^2 b^2 c^2 (z_1 - z_0)^2}{b^2 c^2 (x_1 - x_0)^2 + a^2 c^2 (y_1 - y_0)^2 + a^2 b^2 (z_1 - z_0)^2} \tag{S1.6}$$

So far, it is ready to solve for the equilibrium distance

$$r_0 = \sqrt{(x - x_0)^2 + (y - y_0)^2 + (z - z_0)^2}$$
$$= \sqrt{\frac{a^2 b^2 c^2 \left[(x_1 - x_0)^2 + (y_1 - y_0)^2 + (z_1 - z_0)^2 \right]}{b^2 c^2 (x_1 - x_0)^2 + a^2 c^2 (y_1 - y_0)^2 + a^2 b^2 (z_1 - z_0)^2}} \tag{S1.7}$$

APPENDIX B

MATLAB PROGRAM FOR CONFORMABILITY

This MATLAB program was used to solve for the conformability after deformation. Note that we set the contact tolerance to be 0.035% of the largest displacement of the interconnects.

```
clear,clc
% get nodal coordinates after deformation
node = load('thickness_10.txt');
% read the reference loation of nodes
ref = load ('ref.txt');

num = size(node,1);
% get the largest displacement
dis = 0;
for i = 1:num
   temp = norm(node(i,2:4) - ref(i,2:4));
   if temp > dis
      dis = temp;
   end
end
r = 180; % radius of the substrate
s = 1; % scale factor
dif = dis*3.5e-4; % tolerance
z0 = -180; % center of the substrate
```

```
count = 0;


for i = 1:num
   f = node(i,2)^2/r^2 + node(i,3)^2/r^2 + (node(i,4) - z0)^2/(s*r)^2 - 1;
   if  f < dif
      count = count + 1;
   end
end


% get conformability
c = count/num;
disp('The conformability is: ')
disp(c);
```

APPENDIX C

ABAQUS INPUT FILE

Material in this section gives an example of input file for finite element analysis in commercial package ABAQUS.

```
**Nodal information
*Node
     1,   4.26372766,   61.2456894,          0.
     …
     570,          0.,          0.,         -45.
**Element connectivity
*Element, type=S4R
 1,   1,  59, 410,  68
 …
 379, 406, 397,  49,  58
*Element, type=S3
359, 398,  52, 399
…
373, 569, 407, 408
*USER ELEMENT,NODES=2,TYPE=U1,COORDINATES=3
 1,2,3
*ELEMENT,TYPE=U1,ELSET=TEST1
10000,  570,    1
…
10568,  570,  569
```

```
*UEL PROPERTY,ELSET=TEST1
*Elset, elset=Set-1, generate
1,   379,  1
*Shell Section, elset=Set-1, material=mat1
1,  5
*Material, name=mat1
*Elastic
0.12000,  0.36
*Step, name=Step-1, nlgeom=YES, inc=500000
*Static
1., 0.01, 1e-05, 1.
*Boundary
406, 1, 6
570, 1, 6
*controls,parameters=time incrementation
500000,500000,500000,500000
*End step
```